Systems/Circuits

# Evidence for Layer-Specific Connectional Heterogeneity in the Mouse Auditory Corticocollicular System

Georgiy Yudintsev,[1,3] Alexander R. Asilador,[1,3] Stacy Sons,[1,2] Nathiya Vaithiyalingam Chandra Sekaran,[1,2] Macey Coppinger,[2] Kavya Nair,[2] Masumi Prasad,[2] Gang Xiao,[1,2] Baher A. Ibrahim,[1,2] Yoshitaka Shinagawa,[2] and Daniel A. Llano[1,2,3]

[1]Beckman Institute for Advanced Science and Technology, University of Illinois at Urbana–Champaign, Urbana, Illinois 61801, [2]Department of Molecular and Integrative Physiology, University of Illinois at Urbana–Champaign, Urbana, Illinois 61801, and [3]Neuroscience Program, University of Illinois at Urbana–Champaign, Urbana, Illinois 61801

**The auditory cortex (AC) sends long-range projections to virtually all subcortical auditory structures. One of the largest and most complex of these—the projection between AC and inferior colliculus (IC; the corticocollicular pathway)—originates from layer 5 and deep layer 6. Though previous work has shown that these two corticocollicular projection systems have different physiological properties and network connectivities, their functional organization is poorly understood. Here, using a combination of traditional and viral tracers combined with *in vivo* imaging in both sexes of the mouse, we observed that layer 5 and layer 6 corticocollicular neurons differ in their areas of origin and termination patterns. Layer 5 corticocollicular neurons are concentrated in primary AC, while layer 6 corticocollicular neurons emanate from broad auditory and limbic areas in the temporal cortex. In addition, layer 5 sends dense projections of both small and large (>1 $\mu m^2$ area) terminals to all regions of nonlemniscal IC, while layer 6 sends small terminals to the most superficial 50–100 $\mu m$ of the IC. These findings suggest that layer 5 and 6 corticocollicular projections are optimized to play distinct roles in corticofugal modulation. Layer 5 neurons provide strong, rapid, and unimodal feedback to the nonlemniscal IC, while layer 6 neurons provide heteromodal and limbic modulation diffusely to the nonlemniscal IC. Such organizational diversity in the corticocollicular pathway may help to explain the heterogeneous effects of corticocollicular manipulations and, given similar diversity in corticothalamic pathways, may be a general principle in top-down modulation.**

*Key words:* **auditory cortex; corticocollicular; corticofugal; GCaMP6s; *in vivo* imaging; inferior colliculus**

**Significance Statement**

**We demonstrate that a major descending system in the brain is actually two systems. That is, the auditory corticocollicular projection, which exerts considerable influence over the midbrain, comprises two projections: one from layer 5 and the other from layer 6. The layer 6 projection is diffusely organized, receives multisensory inputs, and ends in small terminals; while the layer 5 projection is derived from a circumscribed auditory cortical area and ends in large terminals. These data suggest that the varied effects of cortical manipulations on the midbrain may be related to effects on two disparate systems. These findings have broader implications because other descending systems derive from two layers. Therefore, a duplex organization may be a common motif in descending control.**

## Introduction

The classical ascending central auditory pathway consists of a series of projections from the auditory brainstem (cochlear nucleus, and superior olivary and lateral lemniscal nuclei) to the inferior colliculus (IC), which projects to the auditory thalamus. The thalamus then projects to the auditory cortex (AC), which has multiple subfields that are interconnected. A prominent feature of the central auditory system is the presence of massive descending connections, which arise virtually at all levels of the auditory pathway (Winer, 2006; Suga, 2008; Malmierca and Ryugo, 2011; Bajo and King, 2013; Terreros and Delano, 2015). One of the largest of these descending pathways, the pathway

Received Oct. 7, 2020; revised Oct. 7, 2021; accepted Oct. 7, 2021.

Author contributions: G.Y., A.R.A., and D.A.L. designed research; G.Y., A.R.A., S.S., N.V.C.S., M.C., K.N., M.P., G.X., B.A.I., Y.S., and D.A.L. performed research; G.Y. and D.A.L. analyzed data; G.Y. wrote the paper.

This work was supported by Department of Health and Human Services | National Institutes of Health | National Institute on Deafness and Other Communication Disorders Grant DC013073 to D.A.L. We thank Dr. Jasmine Grimsley for providing recordings of mouse calls and assistance in their use; and Dr. Hideki Derek Kawai and Dr. Brett Schofield for useful discussions.

M. Coppinger's present address: Department of Microbiology, University of Georgia, Athens, GA 30602.

The authors declare no competing financial interests.

Correspondence should be addressed to Daniel A. Llano at d-llano@illinois.edu.

https://doi.org/10.1523/JNEUROSCI.2624-20.2021

between the AC and IC, referred to here as the corticocollicular system, has recently attracted much attention because of its potential to alter the sensory information processing at the level of the IC. For example, chronic electrical stimulation of frequency-specific regions of the AC evokes long-lasting changes of best frequency representation in the IC in a corticocentric fashion (Yan and Suga, 1998; Yan et al., 2005), while acute stimulation of this pathway diminished stimulus selectivity of IC neurons (Blackwell et al., 2020). In addition to altering the frequency representation, tuning to a number of other sound features including duration, intensity, and location is altered after AC stimulation (Ma and Suga, 2001; Yan and Ehret, 2002; Zhou and Jen, 2005). The corticocollicular system has also been implicated in mediating experience-induced auditory plasticity (Bajo et al., 2010), control of an innate sound-evoked escape behavior (Xiong et al., 2015), and compensatory gain changes following a significant loss of peripheral auditory input (Asokan et al., 2018). Such functional heterogeneity is unlikely to be supported by a single projection type of the corticocollicular neuron, and calls for further understanding and characterization of the anatomy of this projection system. Despite a mounting body of research elucidating the functions of the corticocollicular system, a detailed picture of the functional neuroanatomical organization of this pathway remains to be uncovered.

The auditory corticocollicular projections emanate from distinct regions of layer 5 and lower layer 6 of the temporal cortex. Dual layer 5/layer 6 projections to the IC have been documented across multiple species (Games and Winer, 1988; Künzle, 1995; Coomes et al., 2005; Bajo et al., 2007; Schofield, 2009; Slater et al., 2013), and in the mouse, layer 6 neurons comprise ~20–25% of all corticocollicular neurons (Slater et al., 2019). Neurons from these two layers possess different morphologic, electrophysiological, and local and long-range circuit properties (Slater et al., 2013, 2019; Zurita et al., 2017). In a related descending system, the corticothalamic system, layer 5 and layer 6 projections have been shown to have distinct morphologic, electrophysiological, and network properties (Llano and Sherman, 2008, 2009), and have been hypothesized to have different roles in modulating the thalamus and supporting corticocortical communication (Ojima, 1994; Guillery and Sherman, 2002; Theyel et al., 2010). Whether a similar functional distinction exists between layer 5 and layer 6 corticocollicular projections is not yet known.

One key set of questions regarding layer 5 and layer 6 corticocollicular projections is whether they originate from different regions of the cortex and terminate differentially in the IC. Early neuroanatomical experiments described regional distributions of layer 5 corticocollicular neurons with respect to the IC, but used less sensitive retrograde tracers that did not label the layer 6 pathway (Herbert et al., 1991). In the present study, using sensitive tracers and modern molecular genetic tools to separate layer 5 from layer 6 projections as well as *in vivo* imaging to identify cortical regions, the distributions and cortical regions of origin of layer 5 and layer 6 corticocollicular neurons in the mouse were examined. Substantial heterogeneity and a regional nonoverlap between the corticocollicular neurons arising from the two layers were found. Layer 5 corticocollicular neurons were concentrated over a smaller area of the mouse AC, largely confined to primary regions of the AC, while the areal distribution of layer 6 corticocollicular neurons was wider, extending beyond nonprimary mouse AC regions and into nonauditory limbic regions. In addition, the layer 5 system was found to terminate throughout the nonlemniscal IC in large and small terminals, while the layer 6 system sends small synapses to the most superficial 50–100 μm of the IC. Such neuroanatomical organization would partially explain the functional heterogeneity observed in *in vivo* studies of the corticocollicular system and provides a foundation for forming and testing future hypotheses about this descending projection system.

## Materials and Methods

*Mice.* BALB/c mice, 45–90 d old and of both sexes, were used for most experiments. For mice involving Cre-dependent viruses, Tg(Rbp4-cre)KL100Gsat/Mmucd mice from the Mutant Mouse Resource and Research Center (stock #031125-UCD) or B6.Cg-Foxp2tm1.1(cre)Rpa/J mice from The Jackson Laboratory (stock #030541) were used. For *in vivo* imaging experiments (see details below) and reconstructions, C57BL6J-Tg(Thy1-GCaMP6s)GP4.3DkimJ mice were purchased from The Jackson Laboratory (stock #024275) and bred as heterozygous in the local animal facility. Before the experiments, mice were genotyped in-house (for GCaMP6s and RBP4) or commercially [using Transnetyx (transnetyx.com), for Forkhead box protein P2 (FOXP2)], using the following sequences. For GCaMP6s, forward CATCAGTGCAGCAGAGCTTC, and reverse CAGCGTATCCACATAGCGTA were used. For FOXP2, 13007 Mutant Reverse A IRES, ACACCGGCCTTATTCCAAG, and 36567 Common, TCCGGAGTTAGAAGATGACAGA were used. For RBP4, forward GGGCGGCCTCGGTCCTC, and reverse CGGCAAACGGACAGAAG CATT were used.

*Surgical procedures.* All surgical procedures were approved by the Institutional Animal Care and Use Committee at the University of Illinois at Urbana–Champaign. Mice were housed in animal care facilities approved by the Association for Assessment and Accreditation of Laboratory Animal Care International. Every attempt was made to minimize the number of animals used and to reduce suffering at all stages of the experiments. For Fluoro-Gold injections, animals were anesthetized with ketamine hydrochloride (100 mg/kg) and xylazine (3 mg/kg) intraperitoneally and placed in a stereotaxic apparatus (David Kopf Instruments). Aseptic conditions were maintained throughout the surgery. Fluoro-Gold (Fluorochrome) was either pressure injected or injected into the IC via iontophoresis. For pressure injections, as recommended by the manufacturer (https://fluorochrome.com/flouro-gold/), Fluoro-Gold was dissolved (1%) in distilled water, and 500 nl was pressure injected into the left IC using glass pipettes 10–14 μm in diameter placed into a Nanoject III device. For iontophoretic injections, Fluoro-Gold was dissolved in acetate buffer (0.1 M) at pH 3.4 and injected into the left IC using iontophoresis through a broken glass electrode with 20-μm-diameter tip for 10–15 min at 10 μA positive current, with 7 s on 7 s off (50% duty cycle). These protocols resulted in large unilateral injections into the left IC. Injection sites were checked for spillover to adjacent brain regions and were not included if injection sites spread outside the IC. For injections of red beads to the IC, latex red beads were purchased from Lumafluor and diluted 2:3 in PBS, and 100 nl was injected into the IC using a Nanoject pressure injector. For viral injections to the AC, 1–2% isoflurane in oxygen was used for anesthesia, and animals were placed in a stereotaxic apparatus, as above. Two hundred nanoliters of AAV9 pCAG-FLEX-EGFP-WPRE (catalog #51502, Addgene) or AAV9 pCAG-FLEX-tdTomato-WPRE (catalog #51503, Addgene; titer, $1.9 \times 10^{13}$ viral genomes/ml) was injected 800–1000 μm deep into the AC over a 10–15 min period via a pressure-injector micropipette system, as above.

For *in vivo* imaging, mice were initially anesthetized with a mixture of ketamine and xylazine (same concentrations as above) delivered intraperitoneally using a 27 gauge needle, followed by an intraperitoneal injection of acepromazine (2–3 mg/kg). A skin incision over the dorsal portion of the skull was made, after which the skull was exposed. The dorsal surface of the skull was roughened using a small surgical drill bit. The area was cleaned of any remaining bone pellets, and a small aluminum bolt 1 cm in length was secured to the surface using dental cement (ESPE Ketac, 3M). Once the cement was set, the animal was carried into a dark soundproof chamber for imaging. Proper care was taken to maintain body temperature within the range of 35.5–37°C during imaging

using a direct current temperature controller (FHC) and a rectal thermometer probe.

Upon the completion of each imaging session, Fluoro-Gold was injected into the left IC of these mice, as above. To aid alignment of coronal sections for 3D reconstructions, three fiducial markers were created by iontophoresis of small amounts of tetramethylrhodamine (molecular weight, 10,000 kDa) dissolved in PBS (Thermo Fisher Scientific) into the cortical regions outside the AC. The iontophoretic injections were performed using unbroken glass electrode (tip size, ~0.5 $\mu$m) with 5 $\mu$A positive current and a 7 s 50% duty cycle for 4 min. Using the same filter settings as during *in vivo* imaging, a micrograph of the skull surface and vasculature was taken to aid in coregistration of functional maps with the reconstructions in Neurolucida later. Seven days following the imaging experiment and the surgery, animals were transcardially perfused, after which the brain tissue was processed according to a standard histologic protocol described further below.

*Macroscope and* in vivo *imaging setup.* An Imager 3001 Integrated Data Acquisition And Analysis System (Optical Imaging) was used to image the cortical responses to sound in GCaMP6s mice. A macroscope consisting of 85 mm f/1.4 and 50 mm f/1.2 Nikon lenses was mounted on an Adimec 1000m high-end CCD camera (pixel size, 7.4 × 7.4 $\mu$m; 1004 × 1004 pixels, thus covering a broad area of 7.4 × 7.4 mm). The image was centered above the left AC to ensure that it was in focus, and the focal plane was adjusted to ~0.5 mm below the surface of the exposed skull. Images were collected at 10 frames/s. The temporalis muscle was reflected, and a surgical drill was used to smooth the surface of the insertion site. Blue excitation (450 nm, 30 nm bandpass), green emission (515 nm, long-pass) filters and a 495 DRLP dichroic mirror were used. Imager 3001 VDAQ software controlled the acquisition and stimulus trigger. Ten repetitions of each stimulus were used, and the average response is displayed.

*Acoustic stimulation and analysis.* Acoustic stimuli were generated using a System 3 (Tucker-Davis Technologies) with an RP 2.1 Enhanced Real-Time Processor and delivered via an ES1 Free Field Electrostatic Speaker (Tucker-Davis Technologies), located 8 cm away from the contralateral ear. All imaging experiments were conducted in a soundproof chamber. Five hundred millisecond pure tones of 5, 10, 20, and 30 kHz were used, 100% amplitude modulated at 20 Hz. In another set of experiments, a series of species-specific mouse calls were used as auditory stimuli. The recordings were used by previous investigators (Grimsley et al., 2011, 2016) and made available by this group. In this study, four calls from three major categories were used. Two calls (calls 1 and 2) are from a group of low-frequency stress calls. Another call (call 3) is a medium-frequency stress call, which the animals produce when restrained. The final call used (call 4) is a mating call. All playbacks were sampled at 200 kHz. Calls 1, 3, and 4 are 500 ms in duration, and call 2 is 300 ms. Custom-written MATLAB software was used to obtain $\Delta F/F$ responses to pure tones (5, 10, 20, and 30 kHz) and species-specific mouse calls. In this way, multiple AC regions could be identified. A threshold of 2.5 SDs threshold above baseline fluorescence was used as a cutoff point to display the peaks of neural signals.

*Fluorescence microscopy and reconstructions.* All coronal sections of the brain that contained retrograde labeling were serially photographed using an Olympus IX71 epifluorescence microscope using 5-× 0.15 numerical aperture (NA) objective. These images were then used to create 3-D reconstructions of the left AC, which were done in Neurolucida (MBF Bioscience). For counting cells and to account for the curvature of the temporal cortex, a grid consisting of 12 rectangular bins (bin size, 118,360 $\mu m^2$) was placed throughout images of the cortex in each coronal section, such that all layers of the cortex were covered. The short base of each rectangle was aligned to the gray-white junction of the cortex. As such, the angle of each rectangle was incrementally decreased from 90° in the most ventral regions of the AC to ~45° at the most dorsal portions of the AC. Thus, cells in any particular bin were radially aligned. The rhinal fissure was used as a reference point for grid placement, with 2 bins of the grid being positioned ventral to the rhinal fissure and 10 bins placed dorsal to the rhinal fissure. The same grid was applied to all sections. Confocal pictures were taken on a SP8 UV/Visible Laser Confocal Microscope (Leica). The 488 and 561 nm excitation beams were used for visualizing EGFP and mCherry, respectively. For analysis of terminal size, similar to previous studies (McGonigal et al., 2012; Petrof and Sherman, 2013; Prasad et al., 2020), maximal-intensity projections of stacks of calibrated images were obtained at 63× (1.4 NA) and imported into ImageJ (https://imagej.nih.gov/ij/) for analysis. As in previous analyses of terminal size (Llano and Sherman, 2008), three square regions of area 2500 $\mu m^2$ were placed over each analyzed brain region for sampling. Terminals were traced with the ellipse function in ImageJ, which automatically calculated terminal area. Based on the numerical aperture of our objective (1.4), we estimated the spatial resolution of our microscope to be 0.24 µm (resolution, 0.61 * 561 nm/NA), with 561 nm being the approximate emission wavelength of EGFP. The corresponding area using this value as radius was 0.18 $\mu m^2$. We therefore conservatively estimate the smallest area measurable on our confocal microscope to be 0.20 $\mu m^2$ and only counted those values in this range or above.

For analysis of layer 5 and 6 neuronal cell body distributions, binned cell counts for each layer were exported as Excel spreadsheets. Abercrombie adjustments were done on each layer cell count separately (Abercrombie, 1946). Full-width at half-maximum analysis of neuronal distributions along dorsoventral and rostrocaudal axes was performed. To compute full-width at half-maximum, cell counts for each layer were summed separately along the rows and along the columns to obtain distributions of counts along the dorsoventral and rostrocaudal axes, respectively. A fourth-degree polynomial provided the best fit for each distribution. The peak and full-width at half-maximum measures were obtained for each layer in both dimensions (dorsoventral and rostrocaudal), using the polynomial fit. This analysis was done for each animal separately. For qualitative comparisons, the individual distributions for layers 5 and 6 were imported into MATLAB (MathWorks) and plotted as contour maps.

*Immunohistochemistry.* The mice were first deeply anesthetized with a lethal intraperitoneal injection of ketamine hydrochloride (200 mg/kg) and xylazine (6 mg/kg), and were perfused transcardially with 4% paraformaldehyde in PBS at pH 7.4. Frozen 50 µm sections were cut using a sliding microtome. Before cutting, three fiducial markers were placed in brain tissue along the rostrocaudal axis using a 27 gauge needle dipped into water-insoluble black India ink. The fiducials were placed to ensure alignment of serial coronal sections for reconstructions in Neurolucida. For immunohistochemistry, sections were washed three times for 5 min in PBS, microwaved for 15 s at full power for antigen retrieval, then incubated for 30 min in PBS containing 0.3% Triton-X (PBT) followed by a 30 min blocking step in a 3% serum containing PBT solution. Blocking serum was of same species that the secondary antibody was generated in. Sections were then incubated with corresponding primary antibody overnight in a cold room. For parvalbumin (PV; Sigma-Aldrich), a 1:1000 dilution was used, and for SMI32 (BioLegend), a 1:1500 dilution was used. Secondary antibody was diluted in the serum solution used for the primary wash, and sections were incubated in this solution for 2 h at room temperature. To avoid any spectral overlap with Fluoro-Gold during imaging of the sections, Alexa Fluor 568-conjugated secondary antibody was used (Thermo Fisher Scientific) to reveal SMI32 or parvalbumin immunoreactivity (Thermo Fisher Scientific). Then, the sections were washed in PBS three times for 10 min each, mounted on gelatin-coated slides, air dried in a dark room, coverslipped using fluorescence mounting medium (Vectashield H-1000, Vector Laboratories), and sealed with nail polish.

*Statistical analysis.* Assumption of normality was not made and pairwise differences were analyzed using nonparametric statistical tests. Wilcoxon rank-sum test was used to compare the differences between layer 5 and layer 6 measures of peaks and full-width at half-maximum measures. Mann–Whitney testing was used to compare the corticocollicular terminals sizes from layer 5 versus layer 6 projections. $p$ Values of $<0.05$ were taken as statistically significant.

## Results

### Layer 5 and layer 6 corticocollicular projections are derived from different cortical areas

Fluoro-Gold was injected into the left IC of 10 mice, producing retrogradely labeled corticocollicular neurons in cortical layers 5

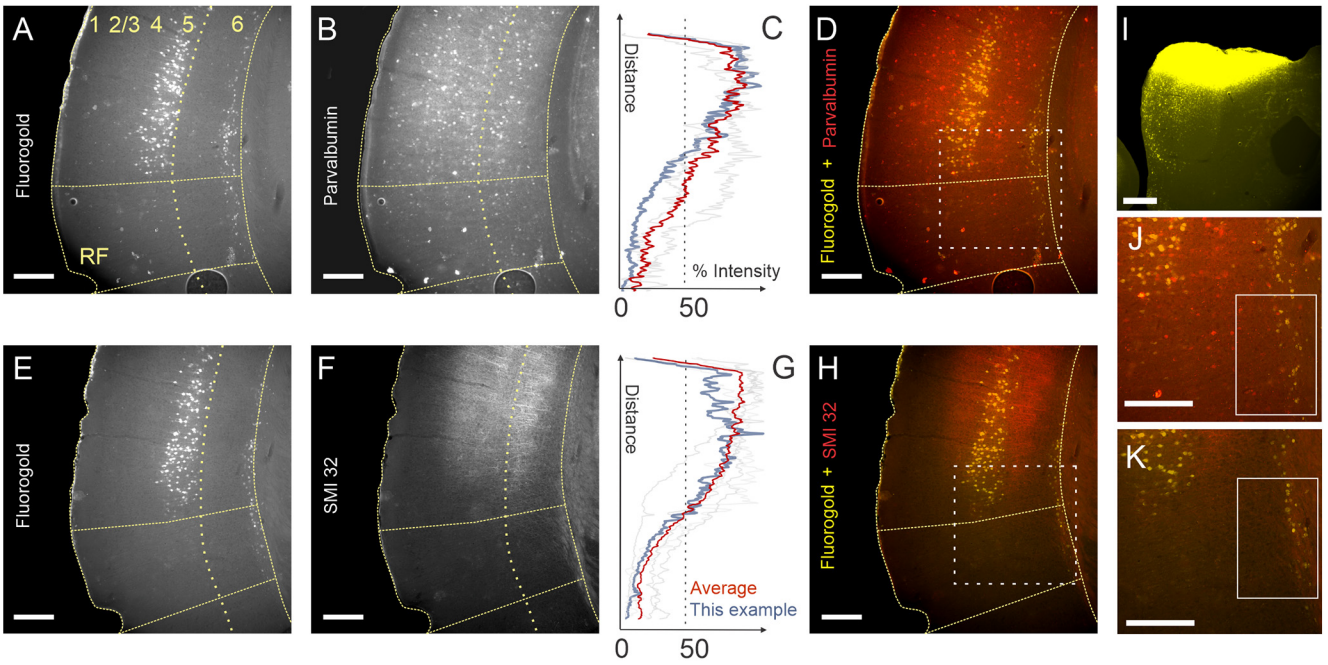


**Figure 1.** Partially segregated distributions of layer 5 and layer 6 corticocollicular neurons in mouse AC. ***A***, ***E***, Corticocollicular neurons in layers 5 and 6 from adjacent coronal sections from the same animal labeled with Fluoro-Gold after an injection into the IC. ***B***, ***F***, Parvalbumin (***B***) and SMI32 (***F***) immunoreactivity in the same sections. ***C***, ***G***, Fluorescence intensity profiles for PV (***C***) and SMI32 (***G***). Blue traces correspond to the intensity of the example mouse shown in this figure. The orange trace is the mean of all animals. Grayed-out traces are the individual other mice from this study. ***D***, ***H***, ***J***, ***K***, Layer 5 corticocollicular neurons are confined to PV- and SMI32-rich regions of the mouse AC (***D***, ***H***), while many layer 6 corticocollicular neurons are found in $PV^{-}$ and $SMI32^{-}$ cortical regions (***D***, ***H***, ***J***, ***K***). ***I***, Corresponding injection of Fluoro-Gold in the left IC. Scale bar, 250 $\mu$m. Dotted boxes in ***D*** and ***H*** correspond to the areas shown in ***J*** and ***K***, respectively. Solid boxes in ***J*** and ***K*** illustrate the presence of layer 6 corticocollicular cells without the presence of corresponding layer 5 corticocollicular cells.

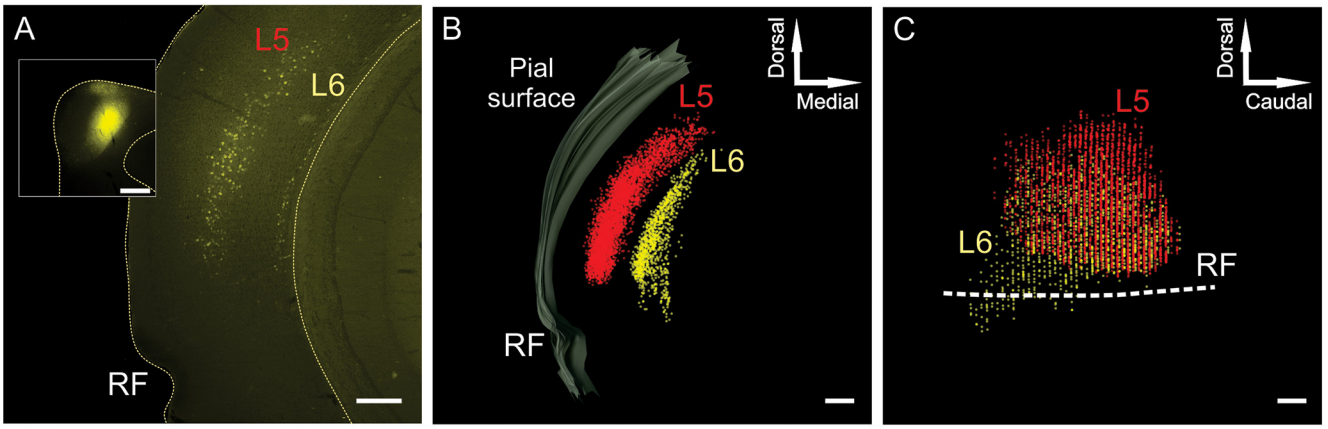


**Figure 2.** A representative reconstruction of corticocollicular cellular distributions in the cortex. ***A***, A representative image of corticocollicular neurons labeled with Fluoro-Gold after IC injection. Images such as this were loaded into Neurolucida, where corticocollicular neurons were marked with a red (layer 5) or a yellow (layer 6) marker, as shown in ***B***. ***B***, A series of pooled reconstructed coronal sections of the mouse brain on the left side. The outer gray border marks the pial surface. ***C***, The results of rotation of this reconstruction by 90° along the *y*-axis results in the lateral view of the reconstructed distributions. Scale bar, 250 $\mu$m.

and 6 in all animals (Fig. 1*A*,*E*). In six cases, the sections were also processed for PV or SMI32 fluorescent immunofluorescence (Fig. 1*B*,*F*). Previous studies reported that PV and SMI32 immunoreactivity in the AC delineate lemniscal auditory areas (primary auditory cortex (A1) and anterior auditory field (AAF; Cruikshank et al., 2001; Horie et al., 2015). However, no studies have described the distribution of layer 5 and 6 corticocollicular neurons with respect to these neurohistological markers. Using a 50% threshold for fluorescence intensity of PV or SMI32 staining (Fig. 1*C*,*G*), it was observed that the majority of layer 5 corticocollicular neurons were restricted to A1 and AAF, while layer 6 corticocollicular neurons, particularly more rostrally, appeared in both PV and SMI32 strongly and weakly stained regions, suggesting that nonlemniscal AC regions are connected with the IC primarily via projection neurons emanating in layer 6 (Fig. 1*D*, *H*,*J*,*K*, insets).

To determine whether layer 5 and layer 6 corticocollicular neurons have different distributions, we first marked the location of all layer 5 and 6 corticocollicular neurons in Neurolucida software so that the retrogradely labeled cells can be visualized in a lateral view, similar to the procedure in the study by Herbert et al. (1991). Micrographs of coronal sections containing corticocollicular neurons were serially aligned and used to create a 3-D reconstruction with plots of layer 5 and 6 corticocollicular cells

(Fig. 2*A–C*). Figure 2 shows the final result of one such reconstruction, where layer 5 corticocollicular cells are represented as red markers, and layer 6 corticocollicular cells as yellow markers. It appeared that layer 5 and 6 corticocollicular cells were substantially nonoverlapping; an area containing layer 6 corticocollicular neurons without any layer 5 corticocollicular neurons was consistently observed rostroventrally (Fig. 2*C*, bottom left, rostrocaudal area showing only layer 6 cells).

For further quantitative analyses, the distributions as shown in Figure 2 were plotted as contour maps. In Figure 3, the rows correspond to individual animals, and the columns contain the injection sites of Fluoro-Gold in left ICs (first column), layer 5 and layer 6 maps of the Fluoro-Gold backlabeled cell bodies (Fig. 3, second and third columns, respectively), and finally the difference between maps for layers 6 and 5 (Fig. 3, fourth column). Here, layer 5 cell counts were subtracted from those for layer 6, and any positive values show regions where the number of layer 6 cells exceeded that in layer 5. Negative values were normalized to zero. This subtraction revealed cortical areas containing larger numbers of layer 6 corticocollicular neurons in each animal. Qualitatively, it appeared that layer 6 corticocollicular neurons occupy overall a broader area in the cortex compared with layer 5 corticocollicular neurons. In each animal, regardless of the IC injection site, an area of nonoverlap with isolated layer 6 corticocollicular neurons was observed rostroventral to the AC (Fig. 3, right-most column). A smaller layer 6-dominant area was also seen dorsocaudally (Fig. 3, rightmost column, rows 2, 5, 6, 7, 8 and 9, top right corners). To quantify these differences in distributions, the widths and peaks of the distribution for layers 5 and 6 within each animal ($n = 10$) were then compared.

The cell counts for each layer and each animal were collapsed in rostrocaudal and dorsoventral axes to obtain two distributions (Fig. 4*A*,*B*). Along the dorsoventral axis, the average full-width at half-maximum for layer 5 was 824.6 $\mu$m (SD = 57.5 $\mu$m), and 929.0 $\mu$m (SD = 92.1 $\mu$m) for layer 6 ($n = 10$; $p = 0.0059$, Wilcoxon signed-rank test; Fig. 4*C*). Along the rostrocaudal axis, the mean value of full-width at half-maximum for layer 5 was 1286.8 $\mu$m (SD = 131.9 $\mu$m), and 1473.7 $\mu$m (SD = 161.9 $\mu$m) for layer 6 ($n = 10$; $p = 0.0020$, Wilcoxon signed-rank test; Fig. 4*D*). Thus, it appears that layer 6 corticocollicular neurons occupy a significantly broader area in the cortex than layer 5, suggesting that these layer 6 neurons may route distinct forms of information from cortical areas surrounding the lemniscal AC areas to the IC. In addition, the peak of layer 5 corticocollicular cells was found to be displaced by 99.9 $\mu$m dorsally and 425.25 $\mu$m caudally relative to layer 6 corticocollicular cells ($n = 10$; $p = 0.0020$, Wilcoxon signed-rank test; Fig. 4*E*), which aligns the peak of the layer 5 corticocollicular distribution with the center of the lemniscal AC areas.

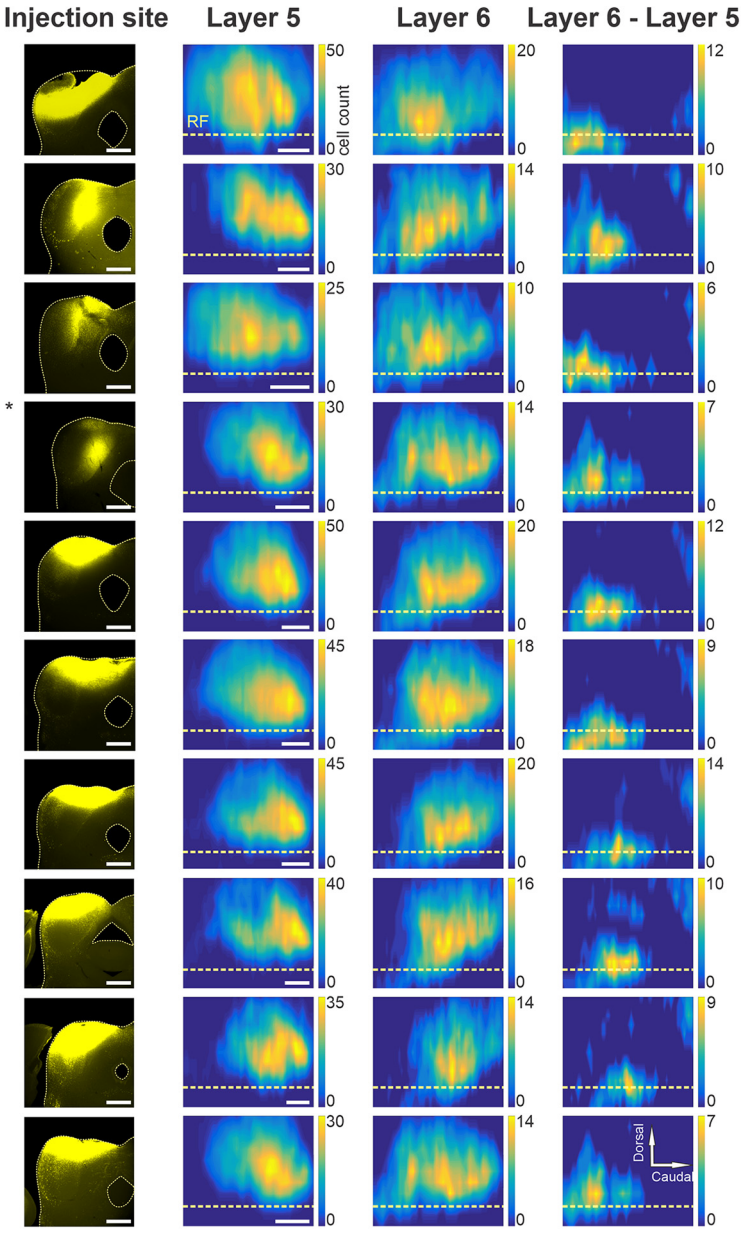


**Figure 3.** Spatial distributions of layer 5 and 6 corticocollicular neurons. Each row includes data from one animal. The first column includes the injection sites of Fluoro-Gold into the left IC of each animal. The second column shows the distribution of layer 5 corticocollicular neurons in the cortex, while the third column has the corresponding distributions of layer 6 corticocollicular neurons. The final column shows the difference (layer 6 – layer 5). The compass in the top right corner describes the directionality for the maps. Scale bar, 250 $\mu$m.

### Rostroventral layer 6 corticocollicular projections are derived from outside of the AC

Given the global anatomic differences between the layer 5 and 6 corticocollicular neuronal distributions described above, we asked whether some of the more rostrally and ventrally located layer 6 corticocollicular cells were in acoustically responsive zones. To answer this question, the left AC in GCaMP6s-Thy1 transgenic mice was mapped by imaging responses to amplitude-modulated pure tones at 5, 10, 20, and 30 kHz using wide-field transcranial optical imaging with blue light (Fig. 5*A–C*). Four auditory subfields could be identified reliably as described by previous investigators (Issa et al., 2014), with A1 and AAF organized tonotopically, converging in high-frequency regions near weakly tonotopic secondary AC (A2). The ultrasonic field (UF) was located dorsally, and only responses to frequencies >20 kHz were present in this field (Fig. 5*C*,*D*). After characterization of the sound-evoked responses, Fluoro-Gold was injected into left IC of these mice, complete reconstructions of layer 5 and 6 corticocollicular distributions were obtained (Fig. 5*E*,*F*), and

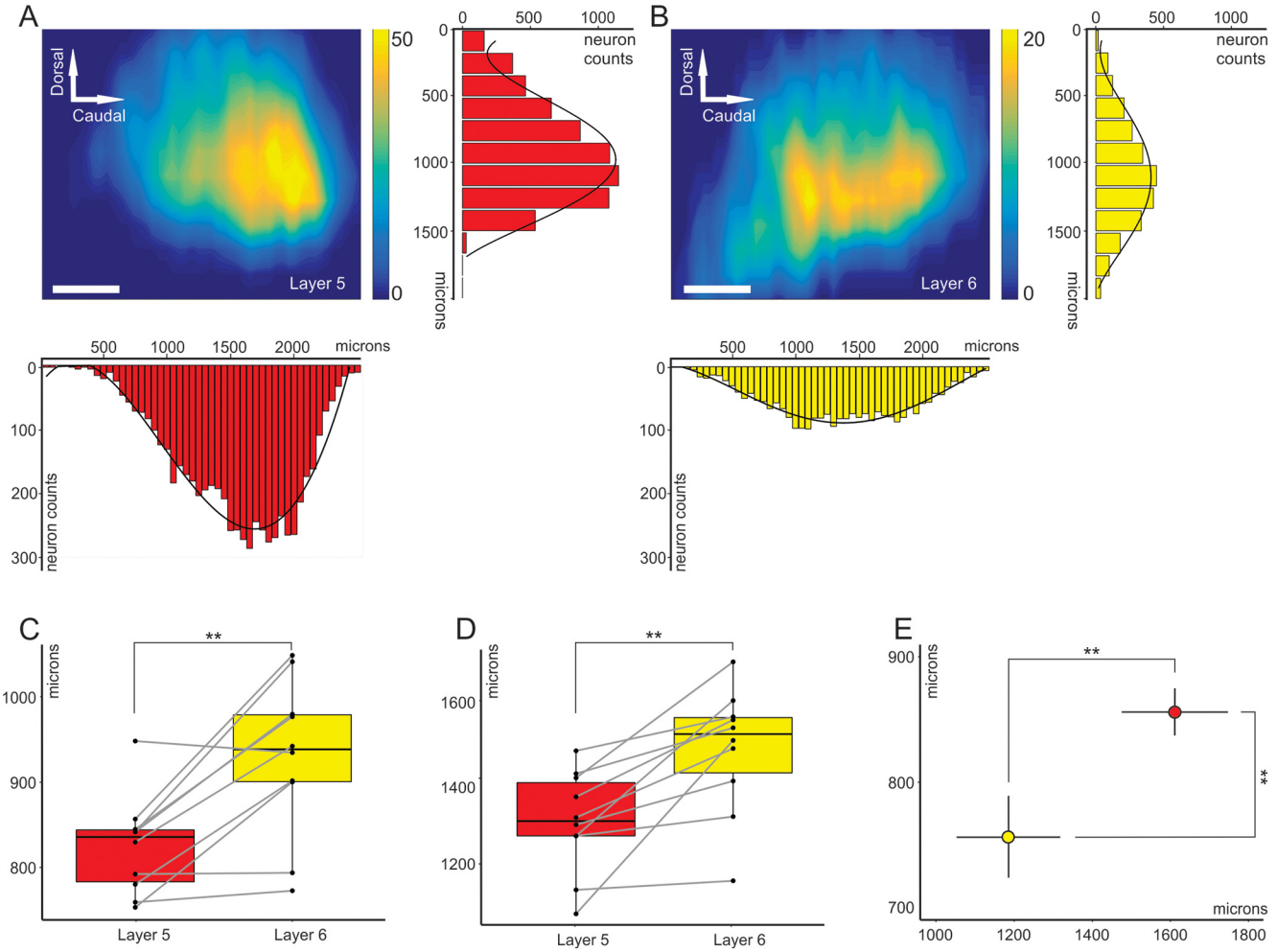


**Figure 4.** Partially segregated distributions of layer 5 and layer 6 corticocollicular neurons in mouse AC. ***A***, Distribution of layer 5 corticocollicular neurons in the neocortex, also showing the summation along the rows, which results in a dorsoventral distribution, and summation along the columns: rostrocaudal distribution. ***B***, Distribution of layer 6 corticocollicular neurons from the same animal. ***C***, Comparison of full-width at half-maximum measures for layers 5 and 6 in the dorsoventral direction (***C***) and rostrocaudal direction (***D***). ***E***, Estimated peaks of layer 5 (red) and layer 6 (yellow) corticocollicular distributions. The peak for layer 6 is shifted more ventrally and rostrally compared with layer 5. The error bars represent 95% confidence intervals. Scale bar, 250 $\mu$m.

previously recorded responses were overlaid with layer 5 and 6 distributions (Fig. 5*G*,*H*).

It was observed that the rostroventral cortical area primarily containing layer 6 corticocollicular neurons appeared outside the main acoustically responsive regions, highlighted with an oval in Figure 5, *G* and *H*. To determine whether this apparently acoustically unresponsive zone would be responsive to more meaningful sounds, the same approach was applied to examine the responses of the AC to ethologically relevant sounds (Grimsley et al., 2011, 2016). Several different species-specific mouse calls were used as stimuli. Again, after obtaining the reconstructions of layer 5 and 6 corticocollicular cells and overlaying these reconstructions with functional mapping, it was found that the rostroventral to AC area enriched in layer 6 corticocollicular cells was outside sound-responsive functional cortical areas (Fig. 6). A similar analysis using white noise as the stimulus revealed similar results (data not shown).

To further characterize this rostroventral region containing isolated layer 6 corticocollicular projections, Fluoro-Gold was injected into this region to label its inputs. Red retrobeads were injected into the IC of the same animal to ensure that the Fluoro-Gold was injected into the nonoverlap area (Fig. 7*A*, injection diagram). Sections were immunostained for PV to ensure that the injection site was in the PV-poor zone of the cortex (Fig. 7*B*, injection site images). The distribution of the inputs from one of these experiments is presented in Figure 7*C*. Consistent with the *in vivo* neuroimaging findings, the rostroventral region received substantial input from nonauditory structures, including the visual and somatosensory cortices, amygdala (LA), parafascicular nucleus (PF), posterior intralaminar nucleus of the thalamus (PIL), lateral posterior nucleus (LP) of the thalamus, mediodorsal nucleus (MD), and posterior complex of the thalamus (PO). Of note, there is essentially no input from the ventral division of the medial geniculate body (MGBv), which is the main lemniscal thalamic nucleus responsible for auditory processing. Similar distributions were seen in $n = 2$ additional mice. These connectivity findings are indicative of the multisensory nature for this cortical area containing isolated layer 6 corticocollicular neurons.

### Layer 5 and layer 6 corticocollicular projections have different termination patterns in the IC

Layer 5 and layer 6 corticofugal neurons have differential patterns of projections in other descending systems such as the corticothalamic pathway (Llano and Sherman, 2008). These anatomic differences are also postulated to have functional

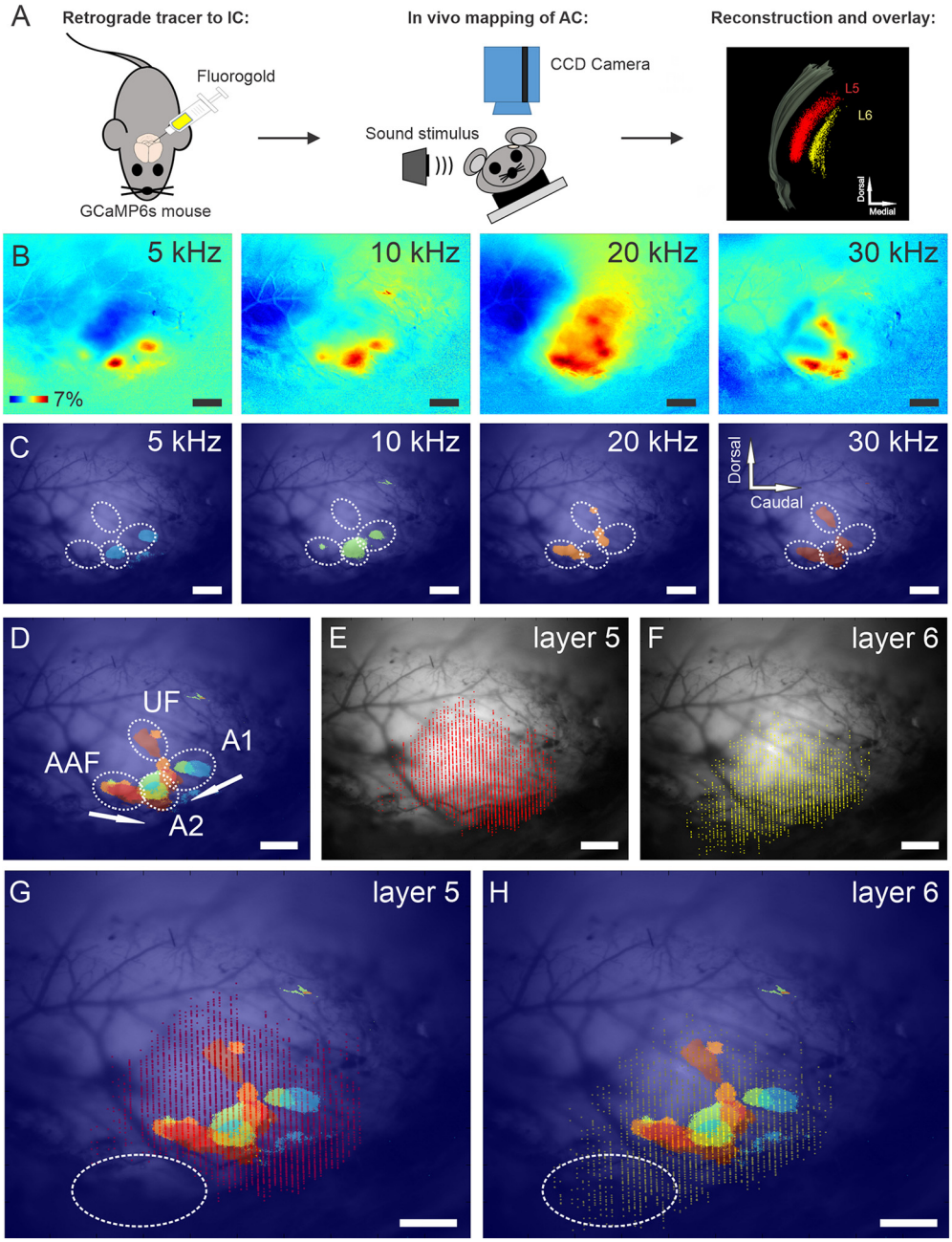


**Figure 5.** Functional maps and corresponding distributions of layer 5 and layer 6 corticocollicular neurons in mouse AC. ***A***, Illustration of experimental design for this figure and Figure 6. GCaMP6s mice were injected with Fluoro-Gold into the IC. The AC of the mice was then mapped using transcranial *in vivo* imaging. The distribution of layer 5 and layer 6 corticollicular neurons was reconstructed using Neurolucida and overlaid on the *in vivo* map. ***B–H***, $\Delta F/F$ responses to 100% amplitude-modulated pure tones in mouse AC (***B***). ***B***, ***C***, A threshold level at 2.5 SDs was set to responses in ***B*** to display the peaks of stimulus-evoked cortical activity (***C***). ***C***, ***D***, Combination of cortical responses at threshold level from ***C*** identifies different auditory regions: tonotopically organized A1 and AAF, as well as A2 and UF (***D***). ***E***, ***F***, Reconstructions of layer 5 (***E***) and layer 6 (***F***) corticocollicular neurons for the same mouse. ***G***, ***H***, Overlays of the tonotopic map and corticocollicular reconstructions. Notice the absence of sound-evoked activity in the rostroventral to AC regions (highlighted in oval). Scale bar, 500 $\mu$m. Sound pressure levels: 5 kHz (70 dB SPL), 10 kHz (30 dB SPL), 20 kHz (29 dB SPL), and 30 kHz (50 dB SPL). $N = 10$ repetitions of each stimulus. Mean responses are displayed.

significance in the forward propagation of sensory information via the higher-order thalamic nuclei (Llano and Sherman, 2009; Theyel et al., 2010). Given the presence of functional neuroanatomical differences with respect to the cortical projections to thalamus, we next aimed to examine the termination patterns of layer 5 and 6 corticocollicular neurons in the mouse IC.

The RBP4-Cre mouse line labels neurons that express retinol-binding protein, which is found in layer 5 corticocollicular neurons (Xiong et al., 2015; Asokan et al., 2018). To confirm this finding and determine the proportion of layer 5 corticocollicular cells that are RBP4+, dual injections of CTb-Alexa Fluor 594 into the IC and a Cre-dependent virus (AAV9 pCAG-FLEX-eGFP-WPRE) into the AC were performed. Similar to the study by Xiong et al. (2015), we found that 77.1% of layer 5 corticocollicular cells (383 of 497) also expressed RBP4 (Fig. 8*A1*,*A2*), suggesting that these cells comprise the majority of the layer 5 corticocollicular projection. Neurons that express FOXP2 in the AC are known to project to the MGB and IC (Chang and Kawai, 2018). We confirmed this finding by injecting Fluoro-Gold into the IC and AAV9 pCAG-FLEX-tdTomato-WPRE into the AC of

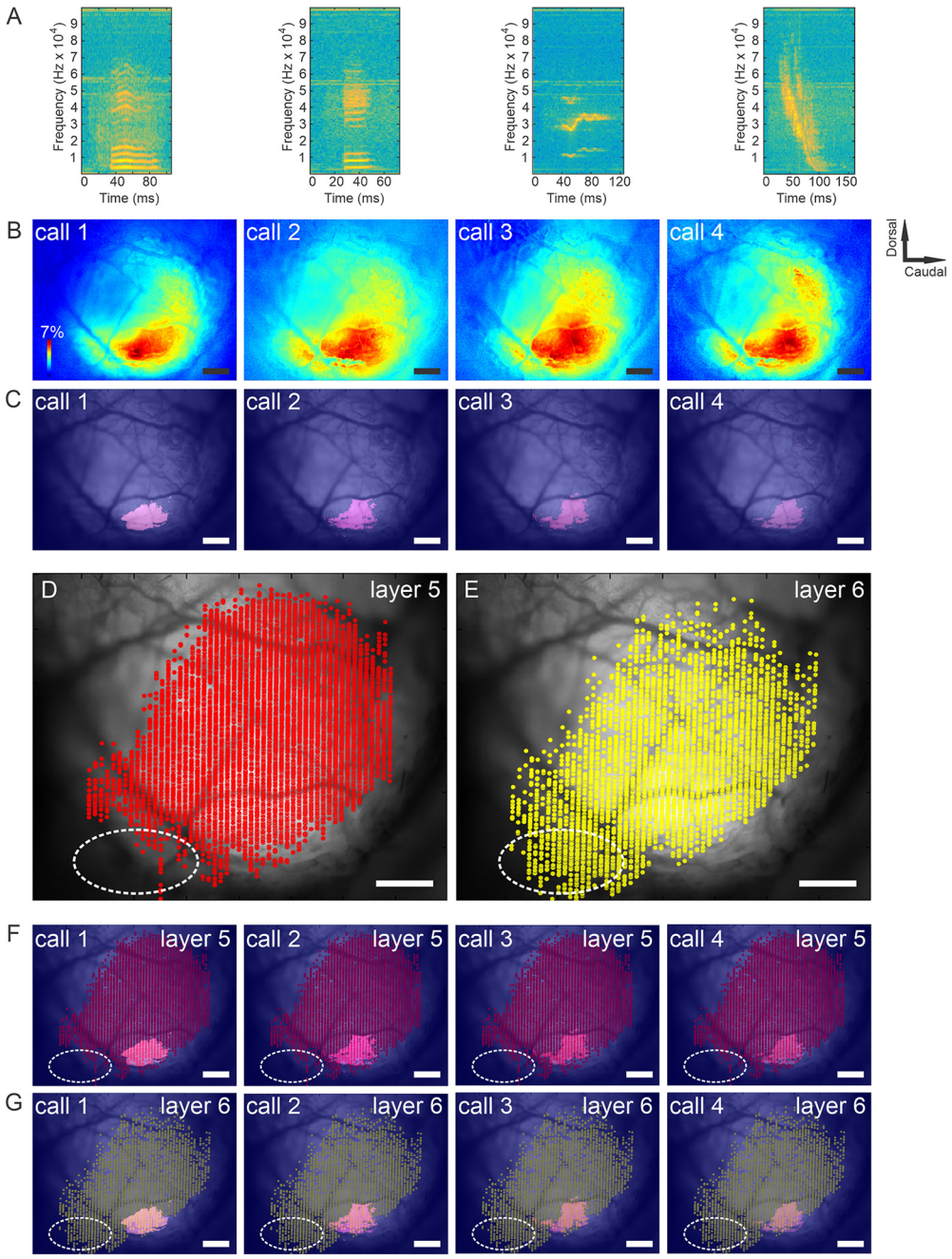


**Figure 6.** Functional responses to ethologically relevant sounds and corresponding distributions of layer 5 and layer 6 corticocollicular neurons in mouse AC. ***A***, Time spectrograms of four classes of mouse calls used in this study. Calls 1 and 2 are low-frequency stress calls, call 3 is a restraint stress-induced medium-frequency call, and call 4 is a mating call. ***B***, $\Delta F/F$ responses to the four classes of species-specific calls. ***C***, ***D***, A threshold level at 2.5 SDs was set to responses in ***A*** (***C***) to display the peaks of stimulus-evoked cortical activity (***D***). ***D***, ***E***, Distributions of layers 5 (***D***) and 6 (***E***) corticocollicular cells. ***F***, ***G***, Overlays of functional maps from ***C*** with layer 5 (***F***) and layer 6 (***G***) corticocollicular cells. Scale bar, 500 $\mu$m. Sound pressure level was ~80 dB SPL for all calls. Sound pressure levels: 5 kHz (70 dB SPL), 10 kHz (30 dB SPL), 20 kHz (29 dB SPL), and 30 kHz (50 dB SPL). $N = 10$ repetitions of each stimulus. Mean responses are displayed.

FOXP2-Cre mice and found that 70% of layer 6 corticocollicular neurons (91 of 130) also expressed FOXP2 (Fig. 8*B1*,*B2*).

The projection patterns of RBP4+ layer 5 corticocollicular neurons and FOXP2+ layer 6 neurons were compared ($n = 2$ mice each). We found that layer 5 corticocollicular projections are found throughout the dorsal cortex of IC (DC) and in layers 1–3 of the lateral cortex of IC (LC) with patchiness in layer 2 (Fig. 8*C1*–*C3*), as previously shown (Lesicko et al., 2016), and were numerically dominant compared with layer 6 terminals. In contrast, layer 6 corticocollicular projections are found primarily along the superficial rim of both the DC and LC (Fig. 8*D1*–*D3*). Both showed relatively weak labeling in the central nucleus of IC. Terminal sizes derived from the two cortical layers were also found to differ. In both DC and LC, average terminal size was significantly larger in layer 5-derived terminals than those from layer 6 (Fig. 8*C3*,*D3*,*E*). Review of their distributions revealed that both had large numbers of terminals $<1$ $\mu m^2$, but that a subset of the layer 5 terminals was larger than this value, while a tiny fraction of the layer 6 terminals were in this range (Fig. 8*F*: 23.2% vs 1.5%, $p < 0.001$, $\chi^2$). Thus, similar to the layer 5 corticothalamic system (Prasad et al., 2020), considerable heterogeneity exists across terminal size in the layer 5 corticocollicular system, though virtually all large terminals were derived from this layer.

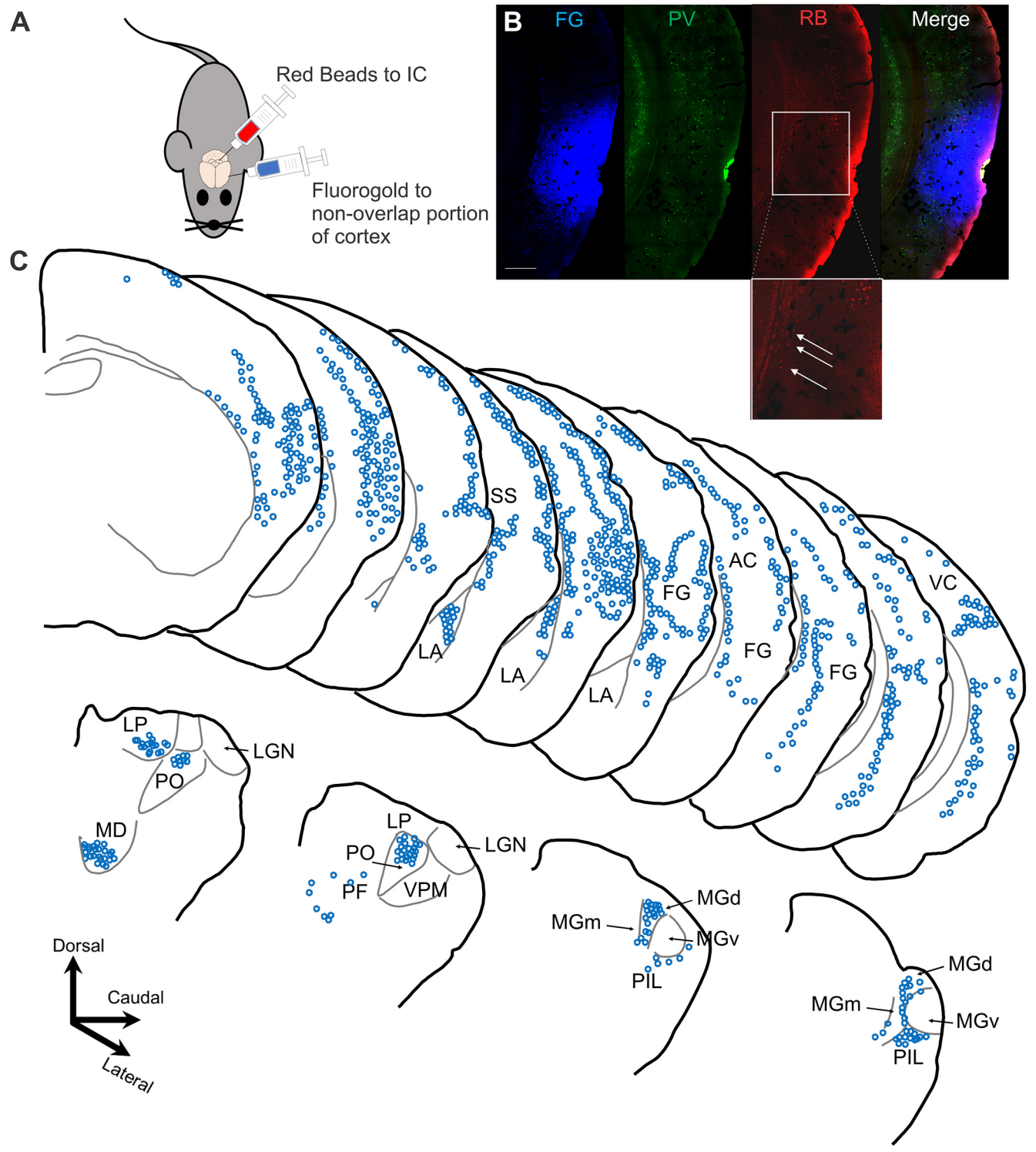


**Figure 7.** Inputs to the cortical area containing layer 6 but not layer 5 corticocollicular neurons. ***A***, Diagram of the dual-injection paradigm, with Fluoro-Gold being injected into the portion of the cortex containing a predominance of layer 6 corticocollicular cells and red retrobeads into the IC. ***B***, The injection site showing Fluoro-Gold, the parvalbumin distributions showing diminished parvalbumin staining in the injection zone, and the red retrobead (RB) distribution. Box and expansion show the region of nonoverlap with layer 6 corticocollicular cells (arrows) without corresponding layer 5 corticocollicular cells. Scale bar, 500 $\mu$m. ***C***, Top, The injection site (FG) and cortical areas where retrogradely labeled neurons were found. A significant portion of inputs came from the lateral nucleus of the LA, as well as somatosensory cortex (SS) and visual cortices (SS and VC, respectively). The bottom panel shows the distribution of neurons in the thalamus and associated structures. The majority of labeled neurons were found in the PO, LP, MD, PIL, and PF, the medial medial geniculate body (MGm), and the dorsal medial geniculate body (MGd), but not the lemniscal MGBv. For display purposes only, Fluoro-Gold is shown in blue.

## Discussion

### Summary of findings

In this study, it was observed that the distributions of layer 5 and layer 6 corticocollicular neurons are partially and significantly nonoverlapping with respect to the cortical areas from which they originate. In particular, layer 6 corticocollicular neurons were derived from a broader area of the cortex than layer 5, and the peak of the distribution of corticocollicular cells shifted more

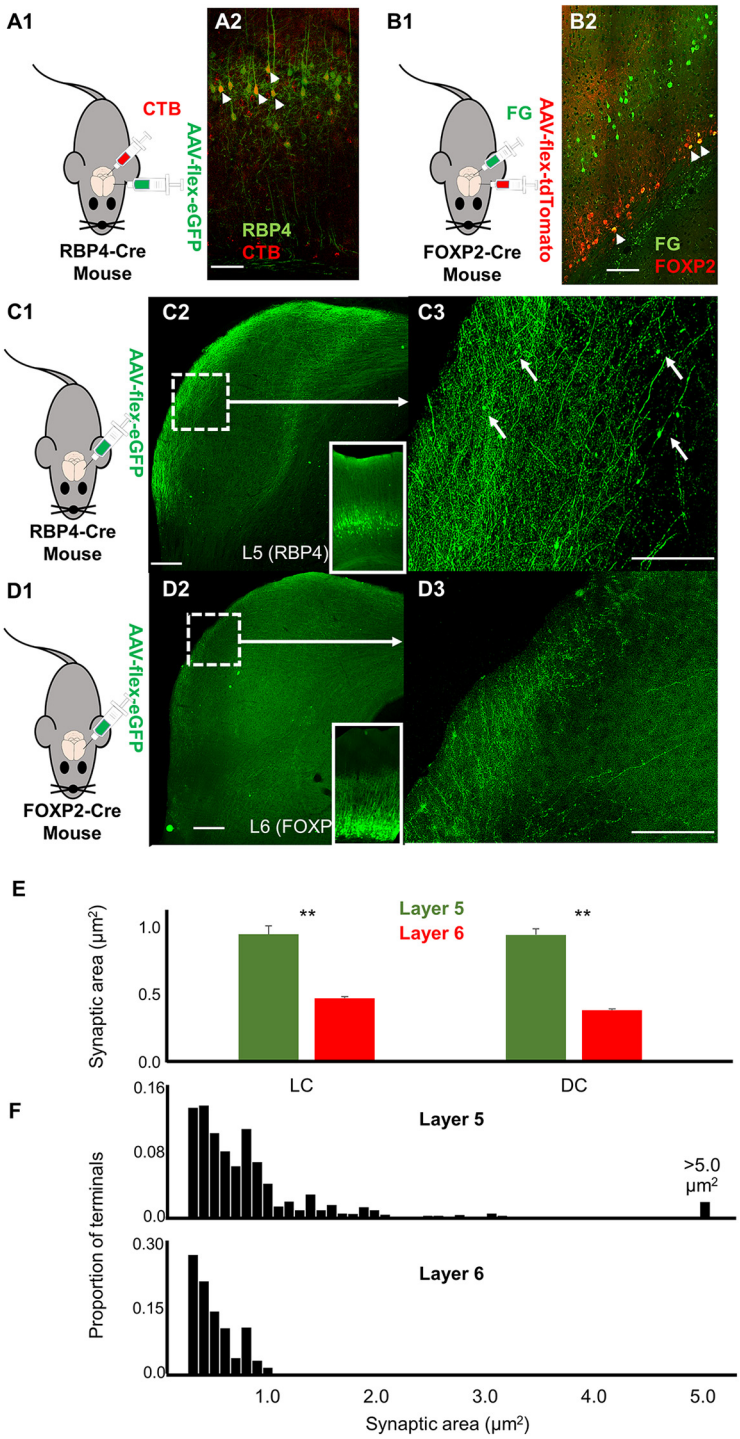


**Figure 8.** Corticocollicular termination patterns at the level of the IC. ***A1***, Diagram illustrating experimental design and validation of use of RBP4-Cre mice to label layer 5 corticocollicular neurons. An RBP4-Cre mouse was injected with CTB-594 to the IC and AAV9-flex-eGFP to the AC. ***A2***, Overlay of CTB-594-labeled corticocollicular cells (red) and RBP4$^+$ cells (green) after AAV9-flex-eGFP injection into the AC showing that a large fraction of layer 5 corticocollicular cells also express RBP4 (small arrows). Scale bar, 100 μm. ***B1***, Diagram illustrating FOXP2-Cre mouse injected with Fluoro-Gold (FG) to the IC and AAV9-flex-tdTomato to the AC. ***B2***, Overlay of Fluoro-Gold-labeled corticocollicular cells (green) and FOXP2$^+$ cells (red) after AAV9-flex-tdtomato injection into the AC showing that a large fraction of corticocollicular cells also express FOXP2 (small arrows). Scale bar, 100 μm. ***C1***, Diagram of experimental design. ***C2***, Low-power micrograph showing EGFP-labeled terminals from an RBP4-Cre mouse with injection of AAV9-flex-eGFP into the AC (injection site at inset). Scale bar, 100 μm. ***C3***, High-power expansion of dotted boxed area from ***A2***. White arrows correspond to large terminals. Scale bar, 50 μm. ***D1***, Diagram of experimental design. ***D2***, Low-power micrograph showing EGFP-labeled terminals from a FOXP2-Cre mouse with injection of AAV9-flex-eGFP into the AC (injection site at inset). Scale bar, 100 μm. ***D3***, High-power expansion of dotted boxed area from ***B2***. Scale bar, 50 μm. ***E***, Mean values for synaptic area for $n = 2$ mice from each group (number of layer 5 terminals in LC, 576; number of layer 6 terminals in DC, 405; number of layer 5 terminals in DC, 824; number of layer 6 terminals in DC, 362). $^{**}p < 0.005$. ***F***, Normalized distributions of terminal sizes (pooled from DC and LC) from layer 5 (top) and layer 6 (bottom). All terminals $<0.2$ μm$^2$ were omitted, given the resolution limits of our microscope.

rostrally and ventrally compared with layer 5. In addition, it was found that the IC receives heavy layer 6 input from nonauditory regions of the cortex, which serves as an indirect conduit to route multisensory and limbic information to the IC. Finally, layer 5 and layer 6 show different termination patterns in the IC with layer 5 sending axons with large terminals distributed throughout the nonlemniscal IC, while layer 6-derived terminals line the most superficial portions of the IC with small terminals. The potential functional implications of these differences are described below.

### Methodological considerations

This study relied on the use of relatively large injections of Fluoro-Gold into the IC to capture a broad range of its cortical inputs. Although it is possible that large injections led to nonspecific labeling of layer 6 neurons, we feel that this is unlikely for a number of reasons. First, the layer 6 inputs were always indexed against those from layer 5, which generally conformed to the known areas of the auditory cortex, based on PV, SMI-32, and GCaMP6 signals. Second, layer 6 is not known to project to any subcortical brain regions other than the thalamus, striatum, claustrum and the IC. Therefore, the only known target in the vicinity of our injections was the IC. Finally, similar results were seen with multiple-sized injections, including iontophoretic injections, suggesting that the results shown were not related to injection spillover.

The findings of this study also suggest that areas of nonauditory cortex send isolated layer 6 projections to the IC. This supposition is based in part on findings that this area does not measurably respond to sound stimuli such as pure tones of different frequencies, and is not responsive to more ethologically relevant sounds such as species-specific calls or to noise. It is possible that imaging the AC in awake animals may have elicited acoustically driven responses from this region. However, the maps elicited in the current study are similar to the distributions of acoustically responsive areas seen in previous studies in awake animals (Issa et al., 2014). It is also possible that other techniques to measure the responsiveness of cortical neurons, such as two-photon imaging, would have revealed acoustically driven responses. Previous work has shown that there is some divergence between what can be measured using single-photon versus

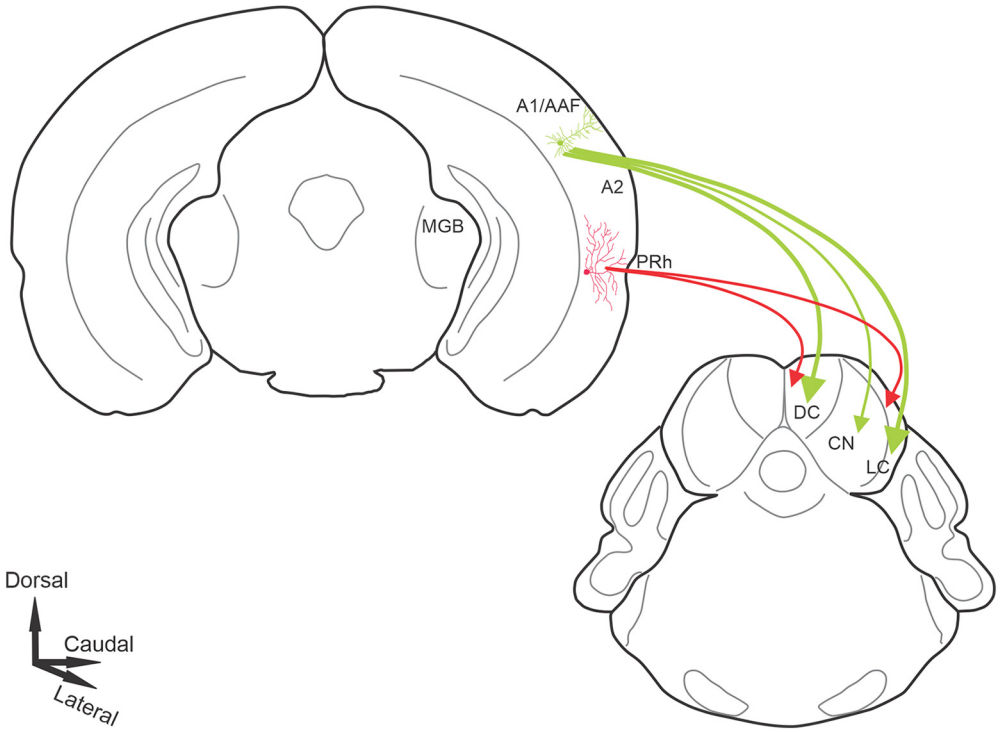


**Figure 9.** Model of layer 5 and layer 6 input to the IC. Pyramidal cells in layer 5 receive direct input from the MGB and send large projections to the nonlemniscal portions of the IC. Nonprimary regions of the AC and nonauditory regions housing layer 6 corticocollicular neurons receive input from nonauditory regions of the thalamus and amygdala. Layer 6 corticocollicular cells then send projections ending in small terminals on the outer rim of the nonlemniscal portions of the IC.

population-based imaging (Bandyopadhyay et al., 2010; Rothschild et al., 2010; Romero et al., 2020). In the current study, four regions of the mouse AC could be distinguished based on their responses to pure tones. A1 and AAF were tonotopically organized, consistent with previous reports (Stiebler et al., 1997; Tohmi et al., 2009; Issa et al., 2014). The ultrasonic frequency pure tones activated neurons in the UF, while all pure-tone stimuli also activated A2, located ventrally to the A1 and AAF gradient convergence. These regions overlapped more so with the distributions of layer 5 corticocollicular neurons, and less with the corticocollicular neurons emanating from layer 6. Four types of mouse-specific calls used in this study activated neurons located primarily in A2. Again, this activation did not overlap with the rostroventral cortical area containing only layer 6, but not layer 5, corticocollicular cells. Finally, the proposal that this region is a multisensory region is supported by the finding that this area did not receive input from the ventral division of the MGB. The latter finding distinguishes this region from the insular auditory field, which received input from the ventral division of the MGB (Sawatari et al., 2011). Instead, intralaminar and heteromodal thalamic nuclei were the main source of thalamic input to this area, in addition to input from the amygdala.

RBP4-Cre and FOXP2-Cre mice were used to label layer 5 and layer 6 corticocollicular projections, respectively. It is possible that the use of these mice only labeled a subset of the projection to the IC of each layer, thus not providing an accurate representation of the projection of each layer to the IC as a whole. We think this is unlikely for two reasons. First, dual-labeling experiments established that the majority of corticocollicular cells in each layer also expressed each marker (RBP4 in layer 5, 77.1%; FOXP2 in layer 6, 70%). Second, the viral injection approach used to determine whether corticocollicular cells express either RBP4 or FOXP2 is likely to underestimate these percentages because it relies on the spatial overlap between the viral injection site and retrogradely labeled corticocollicular cells. Thus, it is likely that data derived from RBP4 and FOXP2-Cre mice provide a representative assessment of the layer 5 and layer 6 projection to the IC, respectively.

### Implications for top-down modulation of the IC

Differences between the layer 5 and 6 corticocollicular distributions found in this study and previous *in vitro* electrophysiological recordings from these neurons point to different plausible functions of these layers in auditory cortical and midbrain processing (Slater et al., 2013, 2019). Consistent with previous findings (Herbert et al., 1991; Budinger et al., 2000; Bajo et al., 2007), in our study layer 5 corticocollicular neurons also appeared to be confined to tonotopically organized lemniscal auditory fields (A1 and AAF), as confirmed by PV and SMI-32 immunostaining and GCaMP imaging. Thus, these corticocollicular neurons may be the main mediators of frequency shifts and changes in duration tuning observed in the IC-on-AC stimulation. The presence of direct thalamocortical connections onto layer 5 corticocollicular cells (Slater et al., 2019), coupled with their tendency to fire in bursts (Slater et al., 2013), and the presence of large, depressing, AMPA-mediated EPSCs in presumed layer 5 corticocollicular synapses (Oberle et al., 2021), now combined with the finding of large synaptic connections, suggest that layer 5 corticocollicular cells can have rapid, powerful, and frequency-specific effects on IC neurons, similar to "drivers" that have been described in the layer 5 corticothalamic system (Sherman and Guillery, 2011).

Unlike layer 5, the nonoverlapping area of layer 6 corticocollicular neurons found rostrally and ventrally may be important for integrating information more broadly than those for layer 5. Based on the comparison of this region to published anatomic atlases, likely candidates for the origin of these projections are the entorhinal and perirhinal cortices (Franklin and Paxinos,

2007; Dong, 2008). In the current study, the lateral nucleus of the amygdala sends a heavy projection to this area, as well as upper-layer neurons found in somatosensory and visual cortices (Fig. 7). These findings suggest that layer 6 corticocollicular neurons are preferentially found in brain regions that funnel a broad spectrum of visual, somatosensory, and limbic information, potentially to modulate IC function in response to multisensory and emotional stimuli. By targeting the most superficial portions of the LC and DC, these layer 6 projections are expected to provide modulatory influence over these regions, possibly via synaptic connections in the form of small synaptic terminals, similar to layer 6 corticothalamic modulators (Llano and Sherman, 2008), to the small neurons in the fibrodendritic capsule surrounding the LC or DC, or the apically oriented dendrites of LC bitufted, pyramidal, or chandelier neurons in these regions (Morest and Oliver, 1984; Faye-Lund and Osen, 1985; Malmierca et al., 2011). The finding that layer 6 may target superficial portions of the LC while layer 5 targets superficial and deep layers may suggest different roles for these projections. In the cerebral cortex, axons targeting superficial layers may provide a contextual or priming signal needed to permit maximal activation by thalamic afferents (Muckli et al., 2015; Roth et al., 2016; Schuman et al., 2021). It is possible, though speculative, that a similar organization occurs in the cortical layers of the IC. Figure 9 shows a schematic representation of a model of layer 5 versus layer 6 corticocollicular termination patterns.

An additional consideration for the interpretation of the current study is the crossed corticocollicular projection. Approximately 10–20% of the mouse corticocollicular projection is to the contralateral IC; this crossed projection is derived from both layers 5 and 6, and both layers 5 and 6 demonstrate substantial contralateral branches (Chandrasekaran et al., 2021). It is not yet known whether the crossed projection is in part derived from nonauditory portions of the cortex. However, the presence of contralateral branching from both layers 5 and 6 suggests that at least part of this crossed layer 6 pathway receives nonauditory input.

### Conclusions

Combined with previous results suggesting that layer 5 and layer 6 neurons are embedded into distinct cortical networks and have different physiological response properties, the current data support the notion that layer 5 and layer 6 neurons send different messages to the IC. The presence of a rapid pathway from the MGBv, directly to layer 5 corticocollicular cells of the primary AC, which then sends a large terminal-based projection to the IC, stands in contrast with a broadly integrative layer 6 pathway with smaller projections and likely slower conduction, producing slower and possibly longer-term modulation of the IC. This type of dual corticofugal system maximizes the efficiency of the organization of corticofugal inputs: a partially overlapping system of descending projections can receive similar sets of inputs, but its outputs to subcortical centers are split into two systems to maximize rapid frequency-specific modulation (layer 5) while allowing simultaneous slower multimodal modulation (layer 6). Further research will test this hypothesis and determine whether it is a general principle of top-down modulatory control.

## References


Abercrombie M (1946) Estimation of nuclear population from microtome sections. Anat Rec 94:239–247.

Asokan MM, Williamson RS, Hancock KE, Polley DB (2018) Sensory overamplification in layer 5 auditory corticofugal projection neurons following cochlear nerve synaptic damage. Nat Commun 9:2468.

Bajo VM, King AJ (2013) Cortical modulation of auditory processing in the midbrain. Front Neural Circuits 6:114.

Bajo VM, Nodal FR, Bizley JK, Moore DR, King AJ (2007) The ferret auditory cortex: descending projections to the inferior colliculus. Cereb Cortex 17:475–491.

Bajo VM, Nodal FR, Moore DR, King AJ (2010) The descending corticocollicular pathway mediates learning-induced auditory plasticity. Nat Neurosci 13:253–260.

Bandyopadhyay S, Shamma SA, Kanold PO (2010) Dichotomy of functional organization in the mouse auditory cortex. Nat Neurosci 13:361–368.

Blackwell JM, Lesicko AM, Rao W, De Biasi M, Geffen MN (2020) Auditory cortex shapes sound responses in the inferior colliculus. Elife 9:e51890.

Budinger E, Heil P, Scheich H (2000) Functional organization of auditory cortex in the Mongolian gerbil (Meriones unguiculatus). III. Anatomical subdivisions and corticocortical connections. Eur J Neurosci 12:2425–2451.

Chandrasekaran N, Deshpande M, Ibrahim B, Xiao G, Shinagawa Y, Llano D (2021) Patterns of unilateral and bilateral projections from layer 5 and 6 of the auditory cortex to the inferior colliculus in mouse. Front Syst Neurosci, in press.

Chang M, Kawai HD (2018) A characterization of laminar architecture in mouse primary auditory cortex. Brain Struct Funct 223:4187–4209.

Coomes DL, Schofield RM, Schofield BR (2005) Unilateral and bilateral projections from cortical cells to the inferior colliculus in guinea pigs. Brain Res 1042:62–72.

Cruikshank SJ, Killackey HP, Metherate R (2001) Parvalbumin and calbindin are differentially distributed within primary and secondary subregions of the mouse auditory forebrain. Neuroscience 105:553–569.

Dong HW (2008) The Allen reference atlas: a digital color brain atlas of the C57BL/6J male mouse. New York: Wiley.

Faye-Lund H, Osen KK (1985) Anatomy of the inferior colliculus in rat. Anat Embryol (Berl) 171:1–20.

Franklin K, Paxinos G (2007) The mouse brain in stereotaxic coordinates, Ed 3. Amsterdam: Elsevier Science.

Games KD, Winer JA (1988) Layer V in rat auditory cortex: projections to the inferior colliculus and contralateral cortex. Hear Res 34:1–25.

Grimsley JMS, Monaghan JJ, Wenstrup JJ (2011) Development of social vocalizations in mice. PLoS One 6:e17460.

Grimsley JMS, Sheth S, Vallabh N, Grimsley CA, Bhattal J, Latsko M, Jasnow A, Wenstrup JJ (2016) Contextual modulation of vocal behavior in mouse: newly identified 12 kHz "mid-frequency" vocalization emitted during restraint. Front Behav Neurosci 10:38.

Guillery RW, Sherman SM (2002) Thalamic relay functions and their role in corticocortical communication: generalizations from the visual system. Neuron 33:163–175.

Herbert H, Aschoff A, Ostwald J (1991) Topography of projections from the auditory cortex to the inferior colliculus in the rat. J Comp Neurol 304:103–122.

Horie M, Tsukano H, Takebayashi H, Shibuki K (2015) Specific distribution of non-phosphorylated neurofilaments characterizing each subfield in the mouse auditory cortex. Neurosci Lett 606:182–187.

Issa JB, Haeffele BD, Agarwal A, Bergles DE, Young ED, Yue DT (2014) Multiscale optical $Ca^{2+}$ imaging of tonal organization in mouse auditory cortex. Neuron 83:944–959.

Künzle H (1995) Regional and laminar distribution of cortical neurons projecting to either superior or inferior colliculus in the hedgehog tenrec. Cereb Cortex 5:338–352.

Lesicko AM, Hristova T, Maigler K, Llano DA (2016) Connectional modularity of top-down and bottom-up multimodal inputs to the lateral cortex of the inferior colliculus. J Neurosci 36:11037–11050.

Llano DA, Sherman SM (2008) Evidence for nonreciprocal organization of the mouse auditory thalamocortical-corticothalamic projection systems. J Comp Neurol 507:1209–1227.

Llano DA, Sherman SM (2009) Differences in intrinsic properties and local network connectivity of identified layer 5 and layer 6 adult mouse auditory corticothalamic neurons support a dual corticothalamic projection hypothesis. Cereb Cortex 19:2810–2826.

Ma X, Suga N (2001) Corticofugal modulation of duration-tuned neurons in the midbrain auditory nucleus in bats. Proc Natl Acad Sci U S A 98:14060–14065.

Malmierca MS, Ryugo DK (2011) Descending connections of auditory cortex to the midbrain and brain stem. In: The auditory cortex (Winer JA, Schreiner CE, eds), pp 189–208. Boston: Springer.

Malmierca MS, Blackstad TW, Osen KK (2011) Computer-assisted 3-D reconstructions of Golgi-impregnated neurons in the cortical regions of the inferior colliculus of rat. Hear Res 274:13–26.

McGonigal R, Tabatadze N, Routtenberg A (2012) Selective presynaptic terminal remodeling induced by spatial, but not cued, learning: a quantitative confocal study. Hippocampus 22:1242–1255.

Morest DK, Oliver DL (1984) The neuronal architecture of the inferior colliculus in the cat: defining the functional anatomy of the auditory midbrain. J Comp Neurol 222:209–236.

Muckli L, De Martino F, Vizioli L, Petro LS, Smith FW, Ugurbil K, Goebel R, Yacoub E (2015) Contextual feedback to superficial layers of V1. Curr Biol 25:2690–2695.

Oberle HM, Ford A, Czarny J, Apostolides PF (2021) Synaptic mechanisms of top-down control by the auditory cortico-collicular pathway. bioRxiv 2021.07.26.453816.

Ojima H (1994) Terminal morphology and distribution of corticothalamic fibers originating from layers 5 and 6 of cat primary auditory cortex. Cereb Cortex 4:646–663.

Petrof I, Sherman SM (2013) Functional significance of synaptic terminal size in glutamatergic sensory pathways in thalamus and cortex. J Physiol 591:3125–3131.

Prasad JA, Carroll BJ, Sherman SM (2020) Layer 5 corticofugal projections from diverse cortical areas: variations on a pattern of thalamic and extrathalamic targets. J Neurosci 40:5785–5796.

Romero S, Hight AE, Clayton KK, Resnik J, Williamson RS, Hancock KE, Polley DB (2020) Cellular and widefield imaging of sound frequency organization in primary and higher order fields of the mouse auditory cortex. Cereb Cortex 30:1603–1622.

Roth MM, Dahmen JC, Muir DR, Imhof F, Martini FJ, Hofer SB (2016) Thalamic nuclei convey diverse contextual information to layer 1 of visual cortex. Nat Neurosci 19:299–307.

Rothschild G, Nelken I, Mizrahi A (2010) Functional organization and population dynamics in the mouse primary auditory cortex. Nat Neurosci 13:353–360.

Sawatari H, Tanaka Y, Takemoto M, Nishimura M, Hasegawa K, Saitoh K, Song WJ (2011) Identification and characterization of an insular auditory field in mice. Eur J Neurosci 34:1944–1952.

Schofield BR (2009) Projections to the inferior colliculus from layer VI cells of auditory cortex. Neuroscience 159:246–258.

Schuman B, Dellal S, Prönneke A, Machold R, Rudy B (2021) Neocortical layer 1: an elegant solution to top-down and bottom-up integration. Annu Rev Neurosci 44:221–252.

Sherman SM, Guillery RW (2011) Distinct functions for direct and transthalamic corticocortical connections. J Neurophysiol 106:1068–1077.

Slater BJ, Willis AM, Llano DA (2013) Evidence for layer-specific differences in auditory corticocollicular neurons. Neuroscience 229:144–154.

Slater BJ, Sons SK, Yudintsev G, Lee CM, Llano DA (2019) Thalamocortical and intracortical inputs differentiate layer-specific mouse auditory corticocollicular neurons. J Neurosci 39:256– 270.

Stiebler I, Neulist R, Fichtel I, Ehret G (1997) The auditory cortex of the house mouse: left-right differences, tonotopic organization and quantitative analysis of frequency representation. J Comp Physiol A 181:559–571.

Suga N (2008) Role of corticofugal feedback in hearing. J Comp Physiol A Neuroethol Sens Neural Behav Physiol 194:169–183.

Terreros G, Delano PH (2015) Corticofugal modulation of peripheral auditory responses. Front Syst Neurosci 9:134.

Theyel BB, Llano DA, Sherman SM (2010) The corticothalamocortical circuit drives higher-order cortex in the mouse. Nat Neurosci 13:84–88.

Tohmi M, Takahashi K, Kubota Y, Hishida R, Shibuki K (2009) Transcranial flavoprotein fluorescence imaging of mouse cortical activity and plasticity. J Eurochemistry 109:3–9.

Winer JA (2006) Decoding the auditory corticofugal systems. Hear Res 212:1–8.

Xiong XR, Liang F, Zingg B, Ji X-y, Ibrahim LA, Tao HW, Zhang LI (2015) Auditory cortex controls sound-driven innate defense behaviour through corticofugal projections to inferior colliculus. Nat Commun 6:7224.

Yan W, Suga N (1998) Corticofugal modulation of the midbrain frequency map in the bat auditory system. Nat Neurosci 1:54–58.

Yan J, Ehret G (2002) Corticofugal modulation of midbrain sound processing in the house mouse. Eur J Neurosci 16:119–128.

Yan J, Zhang Y, Ehret G (2005) Corticofugal shaping of frequency tuning curves in the central nucleus of the inferior colliculus of mice. J Neurophysiol 93:71–83.

Zhou X, Jen PH-S (2005) Corticofugal modulation of directional sensitivity in the midbrain of the big brown bat, *Eptesicus fuscus*. Hear Res 203:201–215.

Zurita H, Rock C, Perkins J, Apicella AJ (2017) A layer-specific corticofugal input to the mouse superior colliculus. Cereb Cortex 28:2817–2833.